Increasing Power Density of Single-phase Power Converter by Reduced Passive Components Volume for Short-time Operation

Kodai Nishikawa
Dept. of Science of Technology Innovation
Nagaoka University of Technology
Nagaoka, Japan
knishikawa@stn.nagaokaut.ac.jp

Keisuke Kusaka
Dept. of Electrical, Electronics, and Information Engineering
Nagaoka University of Technology
Nagaoka, Japan
kusaka@vos.nagaokaut.ac.jp

Jun-ichi Itoh
Dept. of Science of Technology Innovation
Nagaoka University of Technology
Nagaoka, Japan
itoh@vos.nagaokaut.ac.jp

***Abstract*— This paper proposes a design concept of short-time rated ripple current for electrolytic capacitors and the concept method of inductors that accepts a magnetic saturation in order to reduce the volume of passive components. The short-time rated ripple current for DC-link capacitors is determined by the operation time of power converters and the transient temperature rise characteristic of the electrolytic capacitors with the ripple current exceeding the rated current. The relation between the operation time of the power converters and the current value of the electrolytic capacitors is derived by the thermal characteristics of the electrolytic capacitors. The thermal characteristics are obtained by the experiment for the temperature measurement of the element of the electrolytic capacitors. Besides, this paper provides the design concept of the grid-connected inductor from the magnetization characteristic of magnetic materials in order to reduce the size. The effect of the reducing inductor volume by 15% is demonstrated by the calculation with the experimental results.**

Keywords*— Short-time operation, Passive component, Electrolytic capacitor, magnetic saturation, Interconnected inductor

I. INTRODUCTION

Optimization methods of the passive components are crucial for increasing the power density [1–3]. Mainly the power density limit results from the DC-link capacitors in single-phase inverters because the electrolytic capacitors are used as the DC-link capacitors in large-capacity power converters[4]. Some approaches have been proposed in [1–2, 5-7] in order to reduce the DC-link capacitor volume. The volume is reduced by adapting additional circuit in [1-2], and improving control methods in [5]. In [6–7], the optimization methods are proposed by selecting the DC-link capacitors using the capacitors losses or temperature. However, the DC-link capacitors is designed to satisfy the rated ripple current of the capacitors in the conventional methods. Thus, the rated ripple current is the constraint to the volume reduction of the DC-link capacitors especially for the electrolytic capacitors. Besides, the grid-connected inductors is also significant problem in terms of the volume reduction of the power converter. Generally, increasing switching frequency or allowing large output current ripples help to reduce the grid-connected inductor volume. The optimization methods of the grid-connected inductors have been proposed from the perspective of EMC[8-11]. However, a minimization of the inductor volume is limited because the grid-connected inductors are generally designed in the linear region of the magnetization characteristics in order to avoid the saturation of the magnetic cores.

This paper proposes two design methods in order to reduce the passive component volume for the specific power converters, which operate only at the rated power for a short-time, such as uninterruptible power supplies (UPS) and home appliances compressors. The first method is to adapt the design concept of short-time rated ripple current to the electrolytic capacitors. The electrolytic capacitors allow ripple currents exceeding the rated value based on the transient capacitor temperature. The second method is adapting the design concept of the inductor that allows the magnetic saturation. Allowing magnetic saturation leads to increased losses due to the expanded operating range of the magnetic flux density; however, the increase of losses can be accepted due to the short-time operation. The example of the inductor design using the proposed design method is shown to confirm reducing inductor volume. In addition, the operation of the power converter with the inductors that allow a magnetic saturation is experimentally demonstrated. The originality of this paper is providing a design procedure for the power converters operated for a short-time for downsizing.

II. REDUCTION METHOD OF DC-LINK CAPACITOR VOLUME

A. Short-time rated current of electrolytic capacitors

Figure 1 shows the relationship between the ripple current and the temperature rise of the electrolytic capacitors. The temperature rise occurs due to dielectric loss and joule loss on the resistance of terminals or lead wires when a ripple current flows through the electrolytic capacitors. The excessive temperature rise causes failures such as a vent operation due to increasing internal pressure, increasing tan δ, and capacitance reduction. The rated ripple current of the electrolytic capacitor is determined by the allowable temperature rise from a maximum category temperature of the electrolytic capacitors. However, the temperature rise does not exceed the allowable temperature rise when the operation time is sufficiently shorter than several times the thermal time constant. Thus, the electrolytic capacitors allow an excess of the ripple current for the short-time operation (the short-time ripple current). The short-time rated ripple current is determined by considering a transient temperature rise characteristic of the electrolytic capacitors. Here, the equivalent series resistance (ESR), thermal resistance, and thermal time constant are assumed as constant values with the temperature change. The heating value of the electrolytic capacitors is the product of the ESR value and the square of XI_{rated}, where X is the ratio of the flowing ripple current to the rated ripple current. The temperature rises from the ambient temperature to the steady temperature is the product of the heating value and the thermal resistance. Thus, the steady temperature ΔT_{steady} is given by

$$\Delta T_{steady} = X^2 \Delta T_{rated} = R_{ESR} \left(X I_{rated} \right)^2 R_{th} \qquad (1),$$

where ΔT_{reted} is the steady temperature rise when the rated ripple current flows, R_{ESR} is the ESR value at twice the dominant frequency, R_{th} is a thermal resistance from an element of the capacitors to an ambient.

From (1), the temperature rise to the steady-state is X^2 times ΔT_{reted} when a ripple current that is X times the rated value flows. Therefore, the amount of the transient temperature rise ΔT_{rise} is given by

$$\Delta T_{rise} = X^2 \Delta T_{rated} \left\{ 1 - \exp\left(-\frac{\Delta t}{\tau} \right) \right\} \qquad (2),$$

where τ is a thermal time constant, and Δt is an operation time of power converters.

From (2), the allowable ripple current ratio X, which is the ratio of the short-time rated ripple current to the rated ripple current, is given by

$$X = \sqrt{ \left\{ 1 - \exp\left(-\frac{\Delta t}{\tau} \right) \right\}^{-1} \frac{\Delta T_{rise}}{\Delta T_{rated}} } \qquad (3).$$

B. Thermal measurement of electrolytic capacitors

Figure 2 shows the experimental configuration to measure the transient temperature characteristics of the electrolytic capacitors. There are three temperature measurement points for the electrolytic capacitor: the center of the element, the side of the element, and the minus tab. T-type thermocouples are used for temperature measurement. A DC regenerative power supply connected in series with the electrolytic capacitor is used as the power supply as a variable voltage source.

Table 1 shows the experimental conditions. The pulsation voltage of the DC-link capacitor of single-phase power converters is replicated by applying a voltage of 100 Hz AC and DC bias. The ambient temperature is kept constant at 60°C using a constant temperature chamber, assuming that the electrolytic capacitors are used inside a power converter housing. The operable temperature rise is set to ΔT_{rise} = 29°C based on 60°C due to the maximum allowable electrolytic capacitor temperature.

Figure 3 shows the temperature rise characteristics when the ripple current is twice the rated value. The temperature of the minus tab is the highest in the measurement points. The allowable temperature of the minus tab is sufficiently higher than that of the element using an electrolytic solution. The maximum temperature of the minus tab is required to be around 110°C in order to ignore the effect of the heat dissipation from the minus tab on the life of the electrolytic capacitors. Focusing on the temperature rise of the element of capacitors, the temperature at the center of the element is higher than the temperature at the side of the element. This is because that heat dissipation at the center of the element is harder than at the side of the element in spite of the heat generated by the element of the capacitors is uniform. Thus, it is sufficient to consider the temperature rise characteristic of the center of the element, which is the hottest in the element of the capacitors, when considering the short-time rated

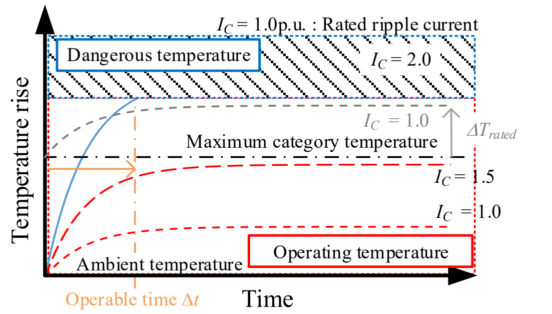

Fig. 1. Relationship between the ripple current and the temperature rise of the electrolytic capacitors.

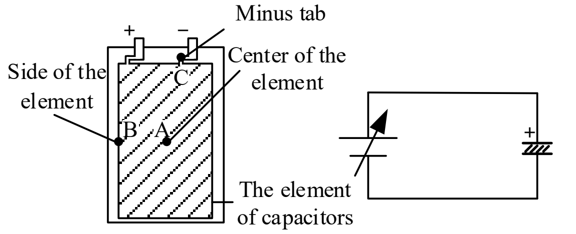

(a) Temperature measurement point (b) Circuit configuration
Fig 2. Experimental configuration to measure capacitor temperature

Table 1. Experimental parameters.

DC bias voltage	V_{dc}	30 V
Applied voltage	V_{sine}	8.1, 16.4, 20.3 V
Applied frequency	f_{sine}	100 Hz
Applied current	I_{sine}	42.7, 85.4, 106.8 A_{rms}
Capacitor: ECSH401LGN123MFH0N NIPPON CHEMI-CON	C	12 mF
Capacitor rated voltage	V_{rated}	400 V
Maximum category temperature	T_{rated}	85°C
Rated ripple current (85°C, ΔT:10°C)	I_{rated}	42.7 Arms
Equivalent Series Resistance(ESR) (60 °C, 100 Hz)	R_{ESR}	2.9 ~ 3.3 mΩ

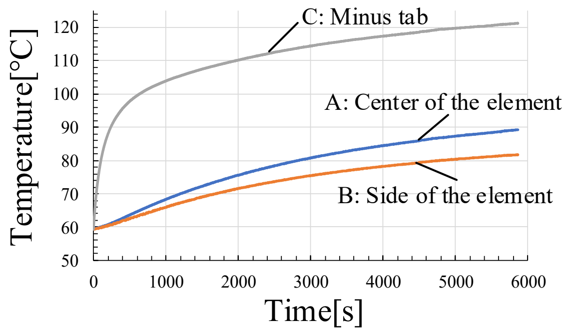

Fig. 3. Capacitor temperature rise characteristics.

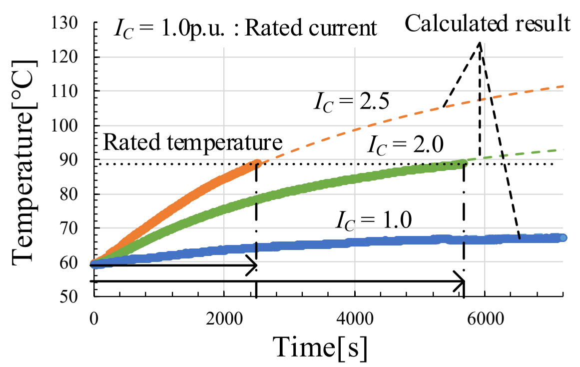

Fig. 4. Temperature comparison between calculated value and measured value.

current and the operable time of short-time operation power converters.

Figure 4 shows measurement results and calculation results of temperature rise characteristics with one time, two times, and 2.5 times the rated current. The thermal time constant in calculation results is set to 4150 seconds calculated from the initial temperature to the 63.2% of steady temperature based on the heat generation test result under the condition of 68 A_{rms} (I_C = 1.6p.u.), 40°C and 120 Hz. The thermal resistance from the center of the capacitor to ambient has been obtained from the slope of the approximate curve by plotting the relationship between the heat generation, which is the product of ESR and a ripple current squared, and the steady temperature. The heat capacity has been calculated from the relation between the thermal time constant and thermal resistance.

According to the temperature rise characteristics, the operable time is 2508 seconds in the measurement result and 2587 seconds in the calculation result, which is about 3% longer than the measurement result with 2.5 times the rated current. Therefore, the derived relationship between the short-time rated current and the operable time is confirmed from the experiment. Error factors in calculation results are that the loss caused by the anodic oxide films of the electrolytic capacitors has temperature dependence.

C. Calculation method of the short-time rated current

The short-time rated current can be obtained by the steady temperature, thermal resistance, and thermal time constant using the heat generation test results for a certain period of time. Thus, doing the heat generation test is not necessary until the time that the temperature rise is saturated. Assuming that ESR, thermal resistance R_{th}, and thermal time constant τ are constant at the time of temperature change, the temperature $T_{\Delta t}$ after Δt seconds derived by the steady temperature T_{steady} and the ambient temperature $T_{ambient}$, is given by

$$T_{\Delta t} = \left(T_{steady} - T_{ambient}\right)\left\{1 - \exp\left(-\frac{t}{\tau}\right)\right\} + T_{ambient} \qquad (4).$$

The following equation is obtained by formula transformation of (4)

$$T_{steady} - T_{\Delta t} = \left(T_{steady} - T_{ambient}\right)\exp\left(-\frac{t}{\tau}\right) \qquad (5).$$

Finding the equation of a natural logarithm on both sides of (5) produces

$$\ln\left(T_{steady} - T_{\Delta t}\right) = \ln\left(T_{steady} - T_{ambient}\right) - \frac{t}{\tau} \qquad (6).$$

The temperature is measured at regular time intervals, $t = t_1$, t_2, t_3, ..., t_n, in the heat generation test. The following equation is obtained from substituting the two adjacent measurement points t_1 and t_2 into (6) to obtain the difference

$$\ln\left(T_{steady} - T_{\Delta t1}\right) - \ln\left(T_{steady} - T_{\Delta t2}\right) = \frac{1}{\tau}\left(t_2 - t_1\right) \qquad (7).$$

Finding the equation of an exponential function on both sides of (7) produces

$$\frac{T_{steady} - T_{\Delta t1}}{T_{steady} - T_{\Delta t2}} = \exp\left(\frac{t_2 - t_1}{\tau}\right) \qquad (8).$$

Furthermore, substituting t_2 and t_3 into (6) to obtain the difference produces

$$\frac{T_{steady} - T_{\Delta t2}}{T_{steady} - T_{\Delta t3}} = \exp\left(\frac{t_3 - t_2}{\tau}\right) \qquad (9).$$

Because the right sides of (8) and (9) are equal, T_{steady} is given by

$$T_{steady} = \frac{T_{\Delta t1}T_{\Delta t3} - T_{\Delta t2}^{\ 2}}{T_{\Delta t1} + T_{\Delta t3} - 2T_{\Delta t2}} \qquad (10).$$

The steady temperature can be obtained from the heat generation test results in a short time by applying (10) to multiple measurement points and finding the average of the calculated T_{steady}. The thermal resistance and thermal time constant can be estimated using the obtained steady temperature average T_{steady_avg}. The thermal resistance R_{th} derived ESR and applied current I_{ripple} is given by

$$R_{th} = \frac{T_{steady}}{R_{ESR} \cdot I_{ripple}^{\ 2}} \qquad (11).$$

The thermal time constant derived by T_{steady_avg}, $T_{ambient}$ and the measured temperature $T_{\Delta tn}$ is given by

$$\frac{t}{\tau} = \ln\left(\frac{T_{steady\_avg} - T_{ambient}}{T_{steady\_avg} - T_{\Delta tn}}\right) \qquad (12).$$

From (12), it can be obtained by substituting the measurement results and calculating the slope by the least-squares approximation since the thermal time constant τ is the reciprocal of the slope.

The instance of the calculation the short-time rated current for an operating time of 10 minutes is shown using the measurement results at 2.5 times the rated ripple current. The steady temperature T_{steady}, thermal resistance R_{th}, the thermal time constant τ are 123.1°C, 1.79 K/W and 3383 seconds using (10), (11) and (12), respectively. The ESR is 3.1 mΩ from table 1. The temperature rise value at the steady temperature with the rated ripple current is ΔT_{rated} = 10.1°C substituting the obtained thermal resistance into (1). Assuming that the allowed temperature rise value is 29°C, the short-time rated current is the current at which ΔT_{rise} = 29°C at Δt = 600 seconds, 10 minutes. The ratio of the short-time rated current to the rated ripple current X derived from (3) is given by

$$X = \sqrt{\left\{1 - \exp\left(-\frac{600}{3884}\right)\right\}^{-1}\frac{29}{10.1}} \approx 4.48 \qquad (13).$$

It can be estimated that the current of 4.48 times the rated ripple current can be accepted as the short-time rated current during a 10-minutes operation.

D. Expected lifetime during the short-time operation

In order to estimate the expected lifetime of the electrolytic capacitors with a short-time operation, it is necessary to estimate the expected lifetimes when the converter is operating and when it is not operating. In [12], an expected lifetime L_X (hours) of a screw terminal type electrolytic capacitor derived by an endurance time L_e, maximum category temperature T_{max}, ambient temperature $T_{ambient}$, temperature rise value with the rated ripple current ΔT_{rated}, acceleration factor of temperature rise value due to the ripple current A, correction factor of an ambient temperature acceleration factor K_t and derating voltage factor K_V is given

$$L_X = L_e \cdot 2^{\frac{K_t(T_{max}-T_{ambient})}{10}} \cdot 2^{\frac{\Delta T_{rated}-\Delta T}{A}} \cdot K_V \quad (14).$$

From (14), the expected lifetimes that the converter is operating L_{X1} and not operating L_{X2} (shelf lifetime) can be estimated. The combined expected lifetime $L_{Xcombined}$ of the combined L_{X1} and L_{X2} derived the ratio of an operation time R_1, the ratio of a non-operation time R_2, L_{X1} and L_{X2} is given by

$$L_{Xcombined} = \frac{1}{\left(\frac{R_1}{L_{X1}} + \frac{R_2}{L_{X2}}\right)} \quad (15).$$

Table 2 shows the example of the condition for the estimation to the combined expected lifetime of the electrolytic capacitors using (14). Substituting the conditions into (14), the expected lifetimes during operation L_{X1} and non-operation L_{X2} are 26,677 hours and 219,230 hours, respectively. Assuming that the operating time is 10 minutes per day, R_1 and R_2 are 0.69% and 99.31%, respectively. The combined expected lifetime $L_{Xcombined}$ is about 23.8 years when calculated by substituting into (15).

III. REDUCTION METHOD OF INTERCONNECTED INDUCTOR VOLUME

A. Design concept of inductors that allow a magnetic saturation

Figure 5 shows the circuit diagram of the grid-tied inverter. The inductance L as the grid-tied inductor is designed under the condition that the allowable ripple current r_I is satisfied at the point where the maximum value of an inverter output current.

Figure 6 shows the magnetization characteristic of the magnetic material used in a design. In this case, the boundary between the linear region and the non-linear region of the magnetization characteristic is approximately 0.9 T. Non-linearity due to a magnetic saturation is expressed by the function $H(B)$, which is a polynomial approximation of the magnetic field H with the magnetic flux density B. The derivative of $H(B)$ is the reciprocal of the magnetic permeability of an iron core μ_C. The effect of air gaps on magnetic permeability is expressed by μ_C and the relationship between an iron core magnetic path l_C and an air gap length l_g. When $l_C >> l_g$, the equivalent magnetic permeability μ_{eq}, which combines the magnetic permeability of the core and the air gap, is given by

$$\mu_{eq} = \left(\frac{1}{\mu_C} + \frac{l_g}{l_C \mu_0}\right)^{-1} = \left(\frac{dH(B)}{dB} + \frac{l_g}{l_C \mu_0}\right)^{-1} \quad (16),$$

where μ_0 is a magnetic permeability in a vacuum.

The integral of the reciprocal of μ_{eq} is the equivalent magnetization characteristic $H_{eq}(B)$. Thus, $H_{eq}(B)$ is given by

$$H_{eq}(B) = H(B) + \frac{l_g}{l_C \mu_0} B \quad (17).$$

Figure 7 shows the shape of the inductor to be designed. It is assumed that the cross-section and the magnetic path of the iron core are square. When $l_C >> l_g$, the volume Vol_L covered rectangular is approximated by

$$Vol_L \approx \left(2\sqrt{A_W} + 2\sqrt{A_C}\right)\left(\sqrt{A_W} + 2\sqrt{A_C}\right)\left(2\sqrt{A_W} + \sqrt{A_C}\right) \quad (18),$$

Table 2. Condition of estimation to the life time with the short-time operation.

	Symbol	The conditions when: The converter is operation	The conditions when: The converter is not operation
The conditions of characteristics of the capacitor	L_e	2000	2000
	T_{max}	85	85
	ΔT_{rated}	10	10
The conditions depending usage environment	$T_{ambient}$	45	45
	ΔT	16.2	0
	K_t	1.09	1.09
	K_V	1	2.67
	A	10	10

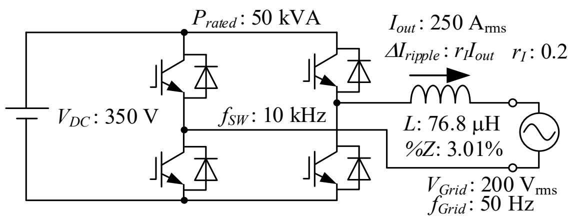

Fig. 5. Single-phase inverter.

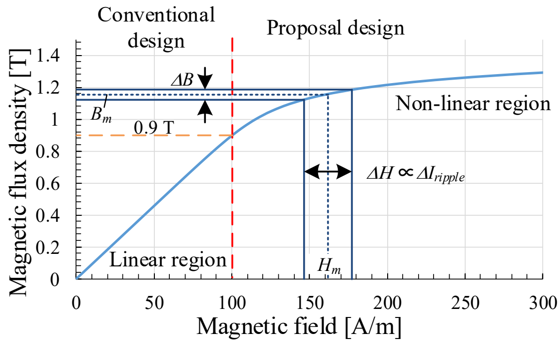

Fig. 6. Magnetization characteristic of the inductor core.

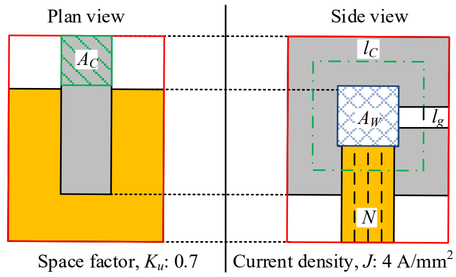

Fig. 7. Configuration of the designed inductor.

where A_C is a cross-sectional area and A_W is a window area of the core. The window area A_W is given by

$$A_W = \frac{I_{out} N}{K_u J} \quad (19),$$

where N is a number of turns of wire, J is a current density of wire, K_u is a space factor of an inductor, I_{out} is an RMS output current value.

The cross-sectional area A_C of the iron core is derived by an allowable magnetic flux density B_m and an allowable ripple current ratio r_I. Assuming that there is no leakage in the magnetic field generated by the inductor winding, the cross-section A_{C1} derived by B_m is given by

$$A_{C1} = \left(\frac{\sqrt{2} I_{out} N}{4H(B_m)} - \sqrt{A_W}\right)^2 \quad (20).$$

The ripple magnetic flux density ΔB corresponding r_I is estimated by $H_{eq}(B)$. The cross-section A_{C2} derived by ΔB is given by

$$A_{C2} = \frac{\sqrt{2}V_{Grid}\left(V_{DC} - \sqrt{2}V_{Grid}\right)}{N\Delta B f_{SW} V_{DC}} \quad (21),$$

where V_{DC} is an input voltage of a DC-AC converter, V_{Grid} is a RMS voltage value of a power grid, and f_{SW} is a switching frequency.

The condition for the inductor to satisfy r_I is $A_{C1} \geq A_{C2}$. Therefore, A_C is determined by the minimum number of N that satisfies this condition.

Figure 8 shows the example of the ripple current value characteristics according to an inductor current phase θ with assuming that a power factor is a unity and an inductance L is constant. From (21), A_{C2} is calculated on the condition that θ = 90 deg. that a sin wave and a magnetic flux density is maximum. Thus, the considering of the ripple current value characteristics is required when the decreasing of inductance by magnetic saturation is a few henries. Assuming a power factor equals one, a ripple current value ΔI_{ripple} derived by V_{DC} and V_{Grid} sin(θ), is given by

$$\Delta I_{ripple} = \frac{\sqrt{2}V_{Grid}\sin(\theta)\left(V_{DC} - \sqrt{2}V_{Grid}\sin(\theta)\right)}{L f_{SW} V_{DC}} \quad (22).$$

From (22), the phase that a ripple current value is maximum θ_{ripple_max} is given by

$$\theta_{ripple\_max} = \sin^{-1}\frac{V_{DC}}{2\sqrt{2}V_{Grid}} \quad (23).$$

From (23), the phase that a ripple current value is maximum θ_{ripple_max} equals 90 deg. on the condition that V_{DC} is higher than $2\sqrt{2}$ V_{Grid}. Thus, using (21) is only required for the calculation of A_{C2} on this condition. On the other hand, the calculation of $A_{C2ripple\_max}$ is required for the considering of a ripple current value characteristic on the condition that V_{DC} is lower than $2\sqrt{2}$ V_{Grid}. From (21), the cross-section $A_{C2ripple\_max}$ is calculated by ΔB_{ripple_max} and $\sqrt{2}$ V_{Grid} sin(θ_{ripple_max}). The ripple magnetic flux density ΔB_{ripple_max} is estimated by r_I, $H_{eq}(B)$ and the inductor current that the phase is θ_{ripple_max}. The additional condition for the inductor to satisfy r_I is $A_{C1} \geq A_{C2ripple\_max}$.

Figure 9 shows the flowchart of the proposed design method. Considered conditions of the method are an allowable magnetic flux density B_m, an air-gap length l_g. Variables are the number of the turn of wire N and the magnetic path length l_{Cref}. The magnetic mean path length l_C is calculated from inductors and variables at the estimated volume. The volume is decided when variables satisfy conditions $A_{C1} \geq A_{C2}$, $A_{C1} \geq A_{C2ripple\_max}$ and $l_{Cref} \approx l_C$.

B. Design Example

The interconnection inductor is designed using the circuit parameters shown in Figure 5.

Figure 10 shows the calculation results of the inductor volume with changing B_m from 0.05 to 2.0 T in 0.05 T increments and lg from zero to 30 mm in 0.5 mm increments. The minimum inductor volume is 2.04 L at B_m = 1.2 T and l_g = 8.5 mm. In contrast, the minimum inductor volume is 2.40 L when a non-liner region of magnetization characteristics (B_m is from 0.95 to 2.0 T) is not used. The proposed design method reduces the inductor volume by 15%

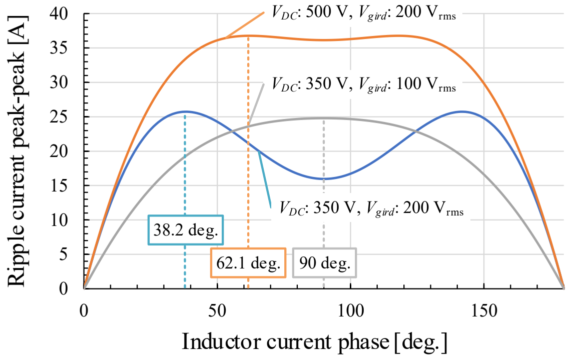

Fig. 8. Ripple current characteristics.

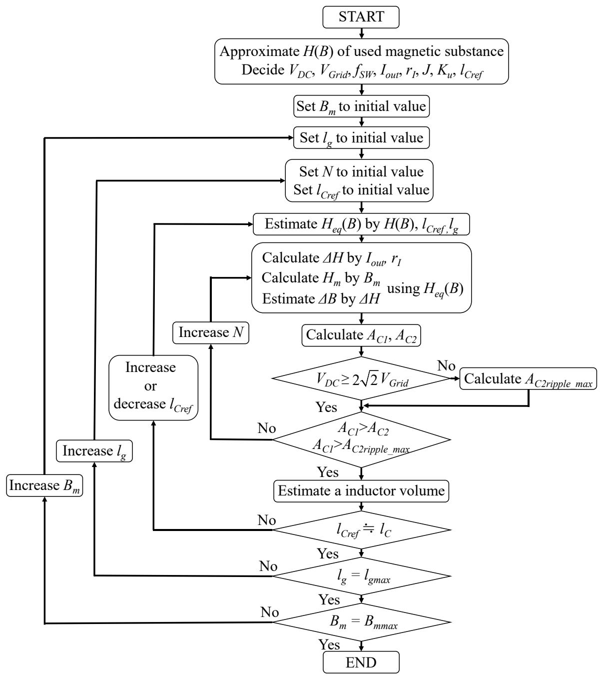

Fig. 9. The flowchat of calculation for inductor volume.

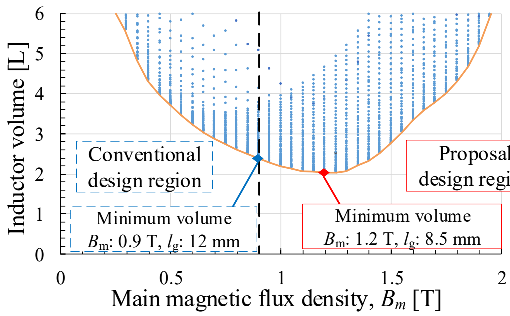

Fig. 10. Results of inductor volume calculation.

C. Experiment with inductors that allowed magnetic saturation

Figure 11 shows the inductance characteristics with the inductor current value i_L used in the experiment. The required inductance conditions of the used inductor are determined to be two types of inductance to satisfy r_I. The first is the required inductance without allowing a magnetic saturation L_{const}. The second is the required inductance with allowing a magnetic saturation on the maximum magnetic flux density $L_{saturated}$. L_{const} is given by

$$L_{const} = \frac{\sqrt{2}V_{Grid}\sin\left(\theta_{ripple\_max}\right)\left(V_{DC} - \sqrt{2}V_{Grid}\sin\left(\theta_{ripple\_max}\right)\right)}{r_I I_{Out} f_{SW} V_{DC}} \quad (24).$$

The inductance $L_{saturated}$ is derived by the inductance characteristic $L_{Volmin}(i_L)$ with the calculated inductor shape conditions that the volume is minimum. The inductance characteristic $L_{Volmin}(i_L)$ derived by the number of turns N_{Volmin}, the magnetic path length l_{C_Volmin}, the cross-section A_{C_Volmin} and the equivalent magnetic permeability with μ_{eq_Volmin}, is given by

$$L_{Volmin}\left(i_L\right) = \frac{N_{Volmin}^2 \mu_{eq\_Volmin}\left(H\left(i_L\right)\right) A_{C\_Volmin}}{l_{C\_Volmin}} \quad (25).$$

where μ_{eq_Volmin} is derived by (16) using the magnetic path length l_{C_Volmin} and the air-gap length l_{g_Volmin}. A magnetic field derived by N_{Volmin} and l_{C_Volmin}, is given by

$$H\left(i_L\right) = \frac{N_{Volmin} i_L}{l_{C\_Volmin}} \quad (26).$$

The inductance $L_{saturated}$ is the range represented by $i_L = \sqrt{2}\, I_{out} \pm 0.5 r_I I_{out}$ in $L_{Volmin}(i_L)$.

Figure 12 shows the output current waveform of the experiment with the inductor that allowed magnetic saturation. The ripple current ratio of the inductor current satisfies the condition. In addition, the total harmonic distortion (THD) of the inductor current is 15.1%. Thus, it is confirmed that the desired ripple current ratio can be satisfied by the appropriate inductance characteristics when the reduction of the inductance due to a magnetic saturation is allowed.

IV. Conclusion

This paper proposes the design concept of short-time rated current for the electrolytic capacitors and the estimation method of inductor volume using magnetic saturation. The temperature measurement in the experiment clarifies the derived relationship between the operable time and the short-time current rating. The result is an error of 3% between the measured and calculated operable times under the condition that the current of 2.5 times the rated current is flowing. Besides, the design example of the inductors that allow a magnetic saturation is shown to demonstrate the effect of the proposed design method. The proposed design achieves the reduction of the inductor volume by 15% compared to the volume of non-magnetic saturation design. In addition, the experimental results shows the THD is 15.1% on the same level with the non-saturated inductor.

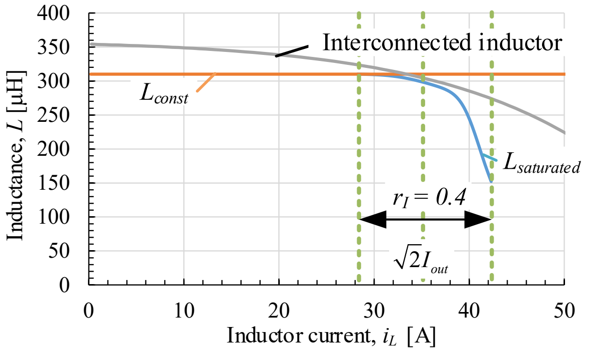

Fig. 11. Inductance characteristics of the interconnected inductor.

Table 3. Experimental parameter.

DC-link voltage	V_{DC}	350 V
Power grid voltage	V_{Grid}	200 V_{rms}
Output current	I_{out}	25 A_{rms}
Switching frequency	f_{SW}	10 kHz
Ripple current maximum phase	θ_{ripple_max}	38 deg.
Required constant inductance	L_{const}	310 μH
Allowable ripple current ratio	r_I	0.4

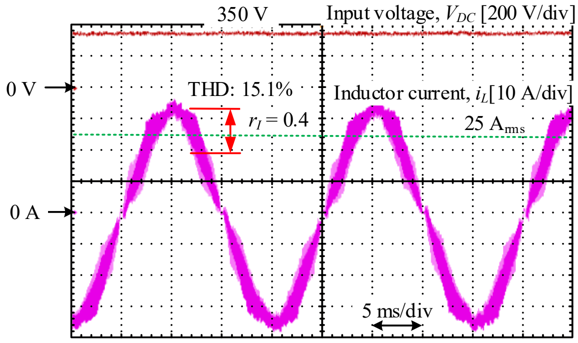

Fig. 12. Inductor current waveform with the inductor that allowed

References

[1] Y. Ohnuma and J. Itoh: "Development of Buck PFC AC-DC Converter using an Active Buffer," IEEJ Journal on Industrial Application, Vol. 133, No. 2, pp. 188-195, February 2013.

[2] Runruo Chen, Yunting Liu and Fang Zheng Peng: "DC Capacitor-Less Inverter for Single-Phase Power Conversion With Minimum Voltageand Current Stress," IEEE Transactions on Power Electronics, Vol.30, No.10 pp.5499-5507, November 2014

[3] K. Park, F. D. Kieferndorf, U. Drofenik, S. Pettersson and F. Canales: "Weight Minimization of LCL Filters for High-Power Converters: Impact of PWM Method on Power Loss and Power Density," IEEE Transactions on Industry Applications, Vol. 53, No. 3, pp.2282 – 2296, May/June 2017.

[4] J.W. Kolar, U. Drofenik, J. Biela, M. Heldwein, H. Ertl, T. Friedli, and S.Round: "PWM Converter Power Density Barriers," IEEJ Journal on Industrial Application, Vol. 128, No. 4, pp. 468-480, April 2008.

[5] B. G. Gu and K. Nam, "A DC-Link Capacitor Minimization Method Through Direct Capacitor Current Control," IEEE Transactions on Industry Applications, Vol. 42, No. 2, March/April 2006

[6] P. Pelletier, J. Guichon, J. Schanen and D. Frey, "Optimization of a DC Capacitor Tank," IEEE Transactions on Industry Applications, Vol. 45, No. 2, March/April 2009.

[7] H. Wen, W. Xiao, X. Wen and P. Armstrong, "Analysis and Evaluation of DC-Link Capacitors for High-Power-Density Electric Vehicle Drive Systems," IEEE Transactions on Vehicular Technology, Vol. 61, No. 7, September 2012

[8] D. O. Boillat, F. Krismer and J. W. Kolar, "EMI Filter Volume Minimization of a Three-Phase, Three-Level T-Type PWM Converter System," IEEE Transactions on Power Electronics, Vol. 3, No. 4, April 2007

[9] M. L. Heldwein and J. W. Kolar, "Impact of EMC Filters on the Power Density of Modern Three-Phase PWM Converters," IEEE Transactions on Power Electronics, Vol. 24, No. 6, June 2009

[10] M. Liserre, F. Blaabjerg and S. Hansen: "Design and control of an LCL-filter-based three-phase active rectifier," IEEE Transactions on Industry Applications, Vol. 41, No. 5, pp. 1281-1291, September 2005.

[11] J. Mühlethaler, M. Schweizer, R. Blattmann, J. W. Kolar, and A. Ecklebe, "Optimal design of LCL harmonic filters for three-phase PFC rectifier," IEEE Transactions on Power Electronics, vol. 28, No. 7, pp. 3114-3125, July 2013.

[12] NIPPON CHEMI-CON, "Technical Note -Judicious Use of Alminum Electrolytic Capacitors-," https://www.chemi-con.co.jp/products /relatedfiles/capacitor/catalog/al-technote-e.pdf